

**Experiment 29****THE MOSSBAUER EFFECT: HYPERFINE SPLITTING**

|  |    |
|--|----|
| INTRODUCTION AND THEORY  | 1  |
| $^{57}\text{Co}$ decay and $^{57}\text{Fe}$ nuclear states.....  | 1  |
| Isomeric shift.....  | 1  |
| Hyperfine splitting: theory.....                                 | 2  |
| Observing hyperfine splitting .....                              | 5  |
| Quadrupole splitting .....                                       | 6  |
| EXPERIMENTAL APPARATUS   | 9  |
| Motion control, source, absorber, detector .....                 | 9  |
| 14.4KeV gamma detection electronics.....                         | 10 |
| Spectrometer unit front-panel controls .....                     | 11 |
| Absorbers.....   | 12 |
| Data capture software .....                                      | 12 |
| EXPERIMENTAL PROCEDURE   | 14 |
| Initial setup.....   | 14 |
| Spectrum acquisitions .....                                      | 15 |
| DATA ANALYSIS  | 16 |
| Channel velocity calibration .....                               | 16 |
| Fitting the absorption lines of a Mössbauer spectrum .....       | 17 |
| Analyzing the absorption line velocities .....                   | 18 |
| Merging the two halves of a spectrum into a single data set..... | 19 |
| PRELAB PROBLEMS  | 20 |



## THE MOSSBAUER EFFECT: HYPERFINE SPLITTING

### INTRODUCTION AND THEORY

Experiment 28 introduced you to the method of using the Mössbauer Effect to enable gamma ray emission and subsequent absorption by nuclei embedded in solid crystals. You obtained an absorption line spectrum of the 14.4keV gamma ray emitted by iron-57 (the daughter nucleus following a cobalt-57 beta decay) and subsequently absorbed by another  $^{57}\text{Fe}$  nucleus situated between the emitter and your gamma ray detector. By Doppler-shifting the gamma ray energy using relative motion of the emitter and absorber, you were able to map out the absorption line spectrum as a function of their relative velocity. The spectrum in that experiment consisted of a single absorption line centered at a source-absorber relative velocity of around  $-0.2\text{mm/sec}$  (emitter and absorber moving away from each other). This so-called *isomeric shift* was caused by the differing chemical compositions of the emitter and absorber crystal matrices, and will be reviewed below.

In this experiment you further investigate this 14.4keV transition in the  $^{57}\text{Fe}$  nucleus. You will discover that both the excited and ground states of this nucleus are *degenerate* (because of the states' angular momenta), and that this energy degeneracy may be *broken* (split) by the ambient electromagnetic field experienced by the nucleus. You will observe as many as six absorption lines in the 14.4keV transition in  $^{57}\text{Fe}$ , as will be described below.

#### $^{57}\text{Co}$ decay and $^{57}\text{Fe}$ nuclear states

The  $^{57}\text{Co}$  beta decay scheme is shown in Figure 1. The gamma ray generated during a transition to the ground state from the 14.413keV excited state of the daughter  $^{57}\text{Fe}$  nucleus is the source photon used to look for absorptions by a target  $^{57}\text{Fe}$  nucleus. Also shown in the figure are the angular momentum quantum numbers of these two nuclear states: in the 14.4keV excited state (denoted by an asterisk, '\*'), the total nuclear angular momentum is  $I^* = 3/2$ , whereas in the  $^{57}\text{Fe}$  ground state  $I = 1/2$ .

#### *Isomeric shift*

The Mössbauer source contains  $^{57}\text{Co}$  atoms embedded in a foil of either rhodium or palladium metal (depending on the manufacturer of the  $^{57}\text{Co}$  radioactive source). In Experiment 28 the

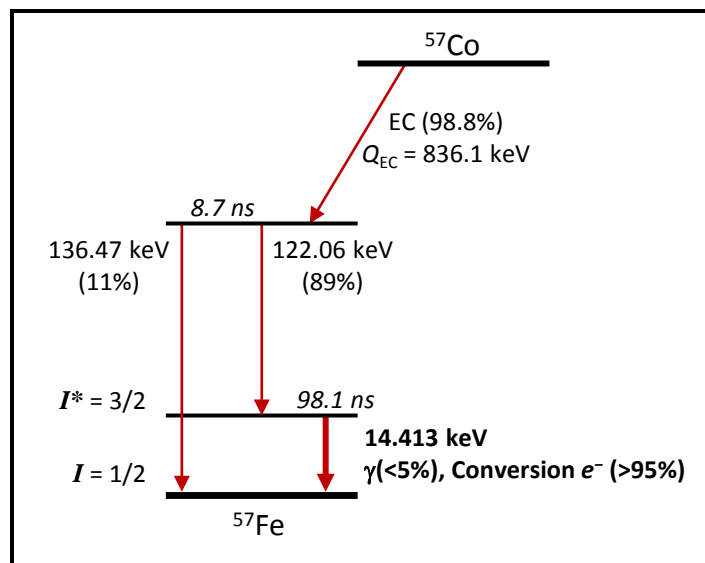


**Figure 1:**  $^{57}\text{Co}$  decay scheme showing the relevant  $^{57}\text{Fe}$  levels and emissions.

absorbing  $^{57}\text{Fe}$  nuclei made up a small fraction of the iron atoms in a thin foil of nonmagnetic stainless steel ( $^{57}\text{Fe}$  makes up about 2.12% of natural iron). The chemical bonds of a  $^{57}\text{Co}$  or a  $^{57}\text{Fe}$  atom to its neighbors in a solid introduce distortions in its various atomic electron wavefunctions. These distortions cause the electromagnetic field surrounding the nucleus to be slightly altered, which in turn very slightly shifts the differences between the energy levels of the nucleon states. These shifts differ for  $^{57}\text{Fe}$  nuclei embedded in different materials, so a slight Doppler shift is required to adjust the emitted gamma energy to that required by the absorber. As discussed in Experiment 28, the small energy shift  $\Delta E$  between source and absorber excitation energies requires a small relative velocity  $v_{\text{iso}}$  to provide a compensating Doppler shift in the emitted gamma ray energy. The required velocity is accurately given by the nonrelativistic formula:

$$\frac{v}{c} = \frac{\Delta E}{E_0} \quad (1)$$

In equation (1)  $E_0 = 14.4\text{keV}$ , and a negative  $\Delta E = E_0(\text{absorber}) - E_0(\text{source})$  requires that the source and absorber move away from each other (red shift,  $v < 0$ ). Typically,  $|\Delta E| \sim 10^{-8}\text{eV}$ , so the shift in energy is in the 11<sup>th</sup> or 12<sup>th</sup> decimal place! By definition,  $^{57}\text{Fe}$  isomeric energy shifts are defined relative to the actual energy of the 14.4keV nuclear transition of  $^{57}\text{Fe}$  when embedded in a crystal of pure, natural iron at room temperature (called  *$\alpha$ -iron*, with a *body-centered cubic* crystal structure). Using numbers for  $c$  and  $E_0$  in (1), the radial velocity  $v$  corresponding to  $\Delta E$  is:

**Energy–velocity relation:** 
$$\boxed{\frac{v}{\Delta E} = 0.208003 \frac{\text{mm/sec}}{10^{-8}\text{eV}}} \quad (2)$$

### ***Hyperfine splitting: theory***

As with an atom's electron states, nuclear states can be expanded in an orthonormal basis of angular momentum eigenstates characterized by two quantum numbers:  $I$  (the total angular momentum quantum number) and  $I_z$  (the “magnetic” quantum number). Each such basis state  $|I, I_z\rangle$  is also an energy eigenstate:  $\mathbf{H}|I, I_z\rangle = E_{I, I_z}|I, I_z\rangle$ . Please note, however, that a state  $|I, I_z\rangle$  may be degenerate, with multiple eigenvalues of the Hamiltonian (energy) operator  $\mathbf{H}$ . In this case, we can (in principle) find another quantum number  $N$  to break this degeneracy, thus

$$\mathbf{H}|N, I, I_z\rangle = E_{N, I, I_z}|N, I, I_z\rangle \quad (3)$$

This situation is analogous, for example, to the case of atomic single-electron eigenstates, where  $N$  is called the *principle quantum number*.

The nuclear states  $|I, I_z\rangle$  are eigenstates of the total angular momentum (squared) operator:  $\mathbf{J}^2|I, I_z\rangle = \hbar^2 I(I+1)|I, I_z\rangle$ . The total angular momentum quantum number  $I$  can take on only nonnegative integer or half-integer values (integers if the number of nucleons is even, half-

integers if the number is odd, as for the case of  $^{57}\text{Fe}$ ). The  $|I, I_z\rangle$  are simultaneously eigenstates of a single angular momentum vector component (traditionally taken to be the  $\hat{z}$  component), so that  $(\hat{\mathbf{z}} \cdot \mathbf{J})|I, I_z\rangle = \mathbf{J}_z|I, I_z\rangle = \hbar I_z|I, I_z\rangle$ . For an eigenstate of  $\mathbf{J}^2$  with quantum number  $I$ , the “magnetic” quantum number  $I_z$  can assume  $(2I+1)$  discrete values with  $-I \leq I_z \leq I$ , and with sequential values of  $I_z$  differing by 1.

For the case of the  $^{57}\text{Fe}$  ground state, the two orthogonal angular momentum eigenstates are

$$|I, I_z\rangle = \left| \frac{1}{2}, \pm \frac{1}{2} \right\rangle.$$

The 14.4keV excited state has 4 angular momentum eigenstates:

$$|I^*, I_z^*\rangle = \left| \frac{3}{2}, \pm \frac{3}{2} \right\rangle \text{ and } |I^*, I_z^*\rangle = \left| \frac{3}{2}, \pm \frac{1}{2} \right\rangle.$$

Nucleons are made up of quarks, each carrying an electric charge. Consequently, nonzero nuclear angular momentum generates an associated nuclear magnetic dipole moment (neutrons as well as protons contribute). The potential energy of this dipole moment in an applied external magnetic field  $\vec{B}$  will shift the energy of a nuclear state (classically by  $\Delta E_B = -\vec{m} \cdot \vec{B}$ ):

**Hyperfine energy shift:**  $\Delta E_B = -m_z B = -g\mu_n I_z B$  (4)

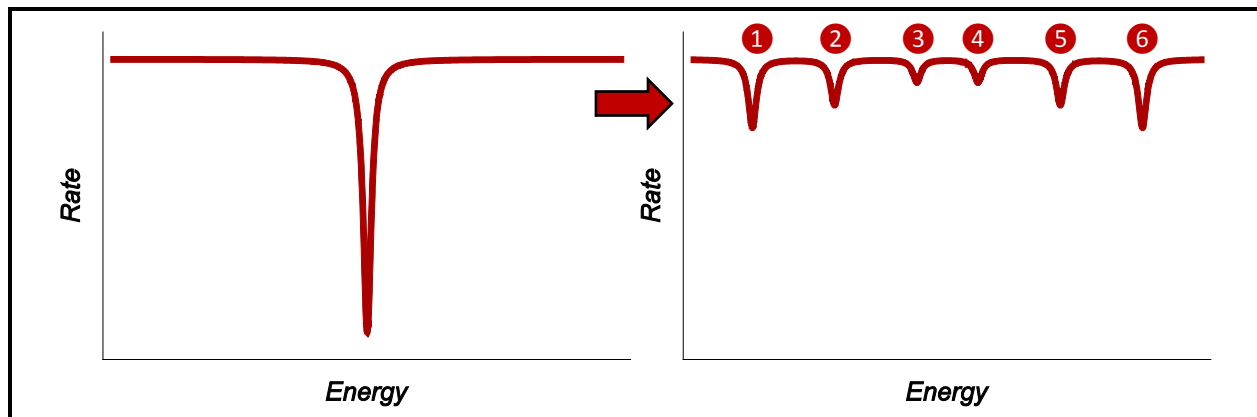
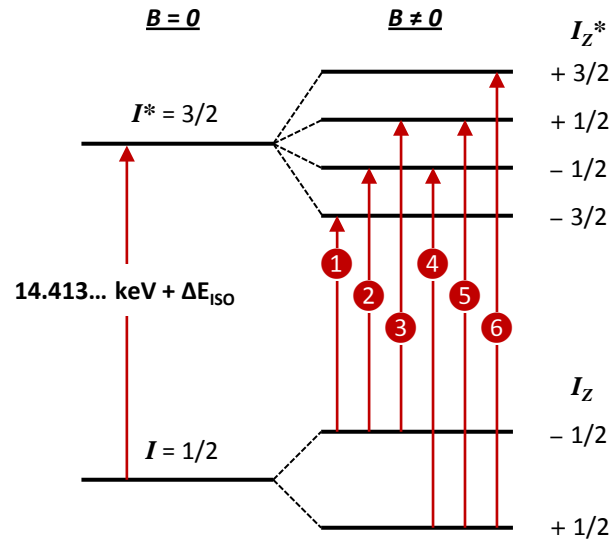
The energy shift (for relatively small field strengths) is proportional to the product of the magnetic flux density  $B$  and the angular momentum component along the direction of  $\vec{B}$ , which is  $\hbar I_z$ . The constant  $\mu_n$  is called the *nuclear magneton*, and is given by:

**Nuclear magneton:**  $\mu_n = \frac{e\hbar}{2m_p} = 3.152451 \times 10^{-8} \text{ eV/Tesla}$  (5)

In equation (5),  $e$  is the proton charge and  $m_p$  is the proton mass. The other constant in equation (4),  $g$ , is called the nuclear state’s *g-factor*, and typically has a value within an order of magnitude or two of unity (if nonzero). It may be positive or negative, and it differs for states of different energies ( $N$ ) and total angular momentum ( $I$ ), but is not otherwise a function of the quantum number  $I_z$ . The ground state of  $^{57}\text{Fe}$  has  $g = +0.18088$ , and, as you will discover for yourself, the ratio of the ground state  $g$ -factor to that of the 14.4keV excited state is  $g/g^* = -1.752$  (note the change in sign, thus  $g^* < 0$ ).

In the presence of an external magnetic field  $B$  the energy of a nuclear state with total angular momentum quantum number  $I$  will therefore split into  $(2I+1)$  energy levels with uniform energy spacing  $g\mu_n B$  between successive levels (since successive levels will have  $\Delta I_z = 1$ ). This *hyperfine splitting* of a nuclear energy level is analogous to Zeeman splitting of atomic energy levels in the presence of an external magnetic field (Experiment 27) and to the *fine structure* of atomic energy levels due to electron spin-orbit coupling. Because the nuclear magneton  $\mu_n$  is approximately 2000 times smaller than the *Bohr magneton*  $\mu_B = e\hbar/2m_e$ , hyperfine splitting of nuclear energy levels can be expected to be much more difficult to observe than the fine structure of atomic electron levels.

Figure 2: Hyperfine splitting of the  $^{57}\text{Fe}$  14.4keV absorption line in the presence of a magnetic field. The change in energy between successive hyperfine levels is given by  $\Delta E = g\mu_n B$ , where the  $g$ -factor differs for the two energy levels:  $g^* \approx -g/1.75$ . Selection rules require that  $\Delta I_z = \pm 1$  or  $0$  for this magnetic dipole gamma-ray transition, leading to the six allowed transitions shown at right and absorption line splitting into the corresponding six lines shown below.



The 14.4keV gamma ray is absorbed by a  $^{57}\text{Fe}$  nucleus via a *magnetic dipole* transition causing, for example, the *spin-flip* of a single nucleon (which has spin  $1/2$ ), changing  $I = 1/2 \rightarrow I^* = 3/2$ , along with  $\Delta I_z = \pm 1$  or  $\Delta I_z = 0$ . These possible changes in  $I$  and  $I_z$  are called *selection rules* for a magnetic dipole transition, because such a transition cannot result in other changes to these quantum numbers. As a consequence of these selection rules, there are six possible transitions between the two ground  $I_z$  states and the four excited  $I_z^*$  states, as shown in Figure 2. This means that the presence of a magnetic field at the nucleus can split the 14.4keV transition into six absorption lines of differing energies.

Note from Figure 2 that the differences in energies (or, equivalently, Doppler velocities using equation (2)) between lines 4 and 2 and between lines 5 and 3 give the hyperfine splitting of the  $^{57}\text{Fe}$  ground state, whereas the energy differences 2-1, 3-2, 5-4, and 6-5 give the splitting of the 14.4keV excited state.

### Observing hyperfine splitting

Hyperfine splitting of the 14.4keV  $^{57}\text{Fe}$  nuclear transition might possibly be observed by placing the absorber sample in the field of a strong electromagnet controlled by the experimenter. Using the measured state  $g$ -factors in equation (4) and with the Doppler shift formula (2), the expected velocity separation of lines 1 and 6 (Figure 2) would be only about 0.32 (mm/sec)/Tesla (see prelab problem 2). With a quantum-limited minimum line width of 0.2 mm/sec (see the notes for Experiment 28), a quite large applied field would be required to clearly separate all six hyperfine lines.

Interestingly, however, an absorber of pure, natural,  $\alpha$ -phase iron, even when not subjected to an experimentally-applied magnetic field, exhibits clearly observable hyperfine splitting, with lines 1 and 6 separated by over 10 mm/sec (see Figure 12 on page 16), corresponding to an applied magnetic field of 33Tesla! Natural metallic iron is *ferromagnetic*: a crystal of iron contains many microscopic domains whose atoms align their magnetic dipole moments all in a single direction (the many domains of a crystal, however, have magnetic moments which are oriented in random directions, unless it is magnetized by an externally-applied field, see Figure 3).

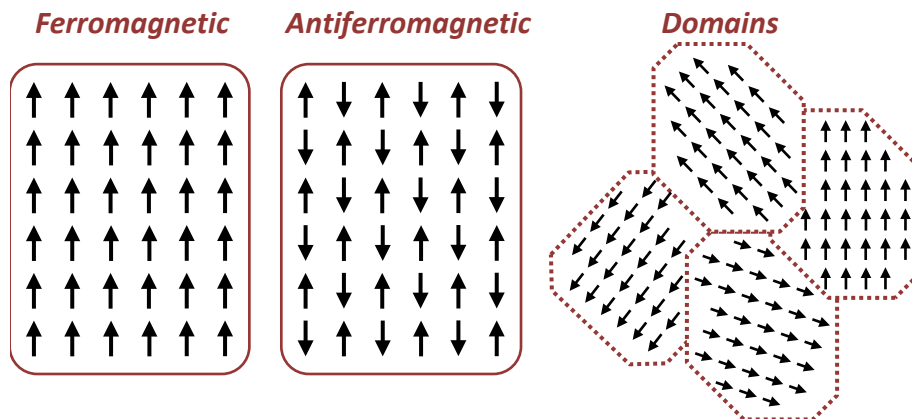


**Figure 3: Ferromagnetic and antiferromagnetic materials exhibit long-range correlations of their atoms' individual magnetic moments (left and center images). These alignments are maintained only over finite, microscopic volumes, however. These volumes, called domains, generally have random orientations relative to each other (right image).**

Each atom in a domain (either ferromagnetic or *antiferromagnetic*, as illustrated in Figure 3) usually has a net magnetic moment equal to a Bohr magneton, generated by a single, unpaired electron's spin. This implies that the ambient *average* magnetic field in a ferromagnetic domain is on the order of a Tesla, much too weak to explain the hyperfine splitting observed in such materials (see Prelab Problem 1). It seems that in these “magnetically active” materials, however, the atomic electrons' wave-functions are so distorted by chemical bonding to neighboring atoms that a single  $s$ -state electron (whose wave-function is nonzero near the nucleus) is left unpaired, and its “naked” magnetic dipole field creates a very large magnetic flux density in the vicinity of

the nucleus. The fields of these  $s$ -state electrons cause the observed hyperfine splitting in  $^{57}\text{Fe}$  nuclei whose atoms are incorporated into ferromagnetic and antiferromagnetic materials.

### *Quadrupole splitting*

Another effect, completely unrelated to hyperfine splitting, is splitting of the 14.4keV transition energy due to the shape of the electrostatic potential well around the nucleus's equilibrium position in the atom. To warm up a bit before attacking the quantum mechanics, first consider the situation of a macroscopic, classical distribution of positive electric charge of finite spatial extent with total charge  $q$  and spatial charge density distribution  $\rho(\vec{r})$ . If this distribution is subject to an independently-generated electric potential  $\phi(\vec{r})$ , then the total electrostatic potential energy  $V$  of the charge distribution *due to only this independent field* would be

$$V = \int \rho(\vec{r})\phi(\vec{r})d^3\vec{r} \quad (6)$$

If the external potential varies slowly over the finite extent of the charge distribution, then we can Taylor expand  $\phi(\vec{r})$  in Cartesian coordinates about the origin:

$$\phi(\vec{r}) = \phi(0) + \vec{r} \cdot \nabla\phi + \frac{1}{2} \sum_{i,j} x_i x_j \frac{\partial^2\phi}{\partial x_i \partial x_j} + \dots$$

Choose the potential at the origin as our reference, so  $\phi(0) \equiv 0$ . The Hessian matrix of second partial derivatives  $\partial^2\phi/\partial x_i \partial x_j$  is clearly symmetric, so we choose Cartesian coordinate axes such that this matrix is diagonal. Substituting our Taylor expansion for  $\phi(\vec{r})$  into the integral (6) for the potential energy  $V$ , we get

$$V = \vec{p} \cdot \nabla\phi + \frac{1}{6} q \sum_i Q_{ii} \left( \frac{\partial^2\phi}{\partial x_i^2} \right) + \dots \quad (7)$$

$$\text{where } \vec{p} \equiv \int \rho(\vec{r}) \vec{r} d^3\vec{r} \quad \text{and} \quad Q_{ii} \equiv \frac{1}{q} \int \rho(\vec{r}) (3x_i^2 - r^2) d^3\vec{r} \quad (8)$$

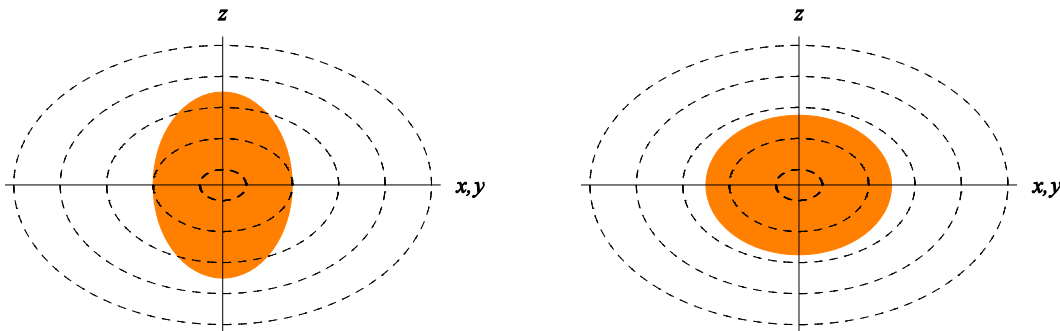


**Figure 4:** Charge distribution in a potential well which is not spherically symmetric, illustrating the quadrupole term in the potential energy, equations (7) and (8). The shaded ellipse represents the charge, the dashed lines contours of an externally-applied electric potential, increasing away from the center (both assumed to be rotationally symmetric about the  $z$ -axis). The charge distribution in the left-hand figure has a total potential energy higher than the one in the right-hand figure.



$\vec{p}$  is the charge distribution's *dipole moment* about the origin ( $\vec{r} = 0$ ), and the three  $Q_{ii}$  defined in (8) are the diagonal elements of the distribution's *traceless Cartesian quadrupole moment tensor* (traceless since  $Q_{xx} + Q_{yy} + Q_{zz} = 0$ ). If the charge distribution is in its equilibrium position at the origin, then the first term for the potential energy in (7) vanishes, and we are left with only the quadrupole term, which depends on the shapes of both the charge distribution and the electrostatic potential well and on their relative orientation (see Figure 4). Note that the  $Q_{ii}$  as defined above have dimensions of *area*.

To extend this classical result into an analogous quantum-mechanical Hamiltonian for the  $^{57}\text{Fe}$  nucleus, consider first the electrostatic potential well within which the nucleus sits. The nucleus has an equilibrium position centered at the bottom of the electrostatic potential well  $\phi(\vec{r})$  established by the atom's electrons. Near the nucleus this well can be written as the sum of two parts: a spherically-symmetric term  $\phi_0(\vec{r})$  modified by the addition of a distortion  $\phi_E(\vec{r})$ :  $\phi(\vec{r}) = \phi_0(\vec{r}) + \phi_E(\vec{r})$ . The spherical symmetry of  $\phi_0(\vec{r})$  ensures that it can make no quadrupole contribution to the nuclear energy in equation (7), so we need only consider the effect of  $\phi_E(\vec{r})$  on the nuclear Hamiltonian. To simplify our problem, we assume that the potential  $\phi_E(\vec{r})$  which distorts  $\phi(\vec{r})$  away from perfect spherical symmetry is rotationally symmetric about the  $z$ -axis, so that its mixed partial second derivatives vanish and  $\partial^2\phi_E/\partial x^2 = \partial^2\phi_E/\partial y^2$ . Now,  $\phi_E$  is caused by electrons relatively far from the nucleus such as atomic electrons with nonzero orbital angular momentum in unfilled subshells or by electrons involved in chemical bonding of the atom to its neighbors in a molecule or crystal. Because  $\phi_E$  is produced by charges external to the nucleus, it must satisfy Laplace's equation near the nucleus:  $\nabla^2\phi_E = 0 = \Sigma(\partial^2\phi_E/\partial x_i^2)$ . Therefore,  $\partial^2\phi_E/\partial x^2 = \partial^2\phi_E/\partial y^2 = -(1/2)\partial^2\phi_E/\partial z^2$ , and the single second partial derivative  $\partial^2\phi_E/\partial z^2$  completely specifies the shape of  $\phi_E$  near the nucleus (up to terms of second order in the Taylor series (7)).

The shape and orientation of the nucleus itself determine its quadrupole tensor components  $Q_{ij}$ . First realize that quantum mechanically, we can't describe the spatial orientation of the nucleus beyond that given by specifying its angular momentum state  $|I, I_z\rangle$ . As for the Cartesian component operators  $\mathbf{Q}_{ij}$  of a quantum-mechanical quadrupole tensor operator  $\mathbf{Q}$ , the unique direction of the  $z$ -axis in the state  $|I, I_z\rangle$  demands that the quadrupole moment tensor operator  $\mathbf{Q}$  be diagonal with  $\mathbf{Q}_{xx} = \mathbf{Q}_{yy}$  (you can picture this condition as arising by imagining that the nucleus is rapidly precessing about the  $z$ -axis). Since  $\mathbf{Q}$  is also traceless, it must be the case that  $\mathbf{Q}_{xx} = \mathbf{Q}_{yy} = -(1/2)\mathbf{Q}_{zz}$ , so the operator  $\mathbf{Q}_{zz}$  uniquely determines the quadrupole tensor  $\mathbf{Q}$ .

Given our symmetry findings and caveats from the above paragraphs, we can now write a quantum mechanical version of the quadrupole energy term in equation (7):

$$\mathbf{H}_Q = \frac{e}{6} \left[ \frac{\partial^2\phi_E}{\partial x^2} \mathbf{Q}_{xx} + \frac{\partial^2\phi_E}{\partial y^2} \mathbf{Q}_{yy} + \frac{\partial^2\phi_E}{\partial z^2} \mathbf{Q}_{zz} \right] = \frac{e}{4} \frac{\partial^2\phi_E}{\partial z^2} \mathbf{Q}_{zz} \quad (9)$$

The various nuclear states  $|I, I_z\rangle$  must be eigenstates of  $\mathbf{Q}_{zz}$ , the quantum-mechanical equivalent of the integral for  $Q_{zz}$ , since it involves only the  $z$ -coordinate and  $r^2$ .  $\mathbf{Q}_{zz}$  must therefore be expressible using only angular momentum operators  $\mathbf{J}^2$  and  $\mathbf{J}_z$ . In fact, the integral of  $3z^2 - r^2$  in (8) must go over into a simple multiple of the quantum operator  $3(\mathbf{J}_z)^2 - \mathbf{J}^2$ . we set the scale of this operator's eigenvalues by first assuming that we can determine the eigenvalue  $Q$  of  $\mathbf{Q}_{zz}$  for the state with maximum  $I_z$ :  $\mathbf{Q}_{zz}|I, I_z = I\rangle = Q|I, I\rangle$ . With this eigenvalue in hand,  $\mathbf{Q}_{zz}$  operating on the other  $|I, I_z\rangle$  states becomes:

$$\mathbf{Q}_{zz} = \frac{Q}{I(2I-1)\hbar^2} \left[ 3(\mathbf{J}_z)^2 - \mathbf{J}^2 \right]$$

with eigenvalues: 
$$\mathbf{Q}_{zz}|I, I_z\rangle = Q \left[ \frac{3I_z^2 - I(I+1)}{I(2I-1)} \right] |I, I_z\rangle \quad (10)$$

The strange-looking denominator  $I(2I-1)\hbar^2$  has been chosen so that  $\mathbf{Q}_{zz}|I, I\rangle$  does indeed equal  $Q|I, I\rangle$ , as required. Clearly, the eigenvalues (10) are undefined if  $I = 0$  or  $I = 1/2$ . It can be shown, however, that  $\mathbf{Q}$  must vanish for these two total angular momentum states. The convention adopted for nuclear quadrupole moments is to use the proton charge  $e = q$  in equations (8) and (9). With dimensions of area,  $Q$  is then quoted in *barns* (1 barn  $\equiv 10^{-28} \text{m}^2$ ). For the 14.4keV excited state of  $^{57}\text{Fe}$ ,  $Q = +0.082$  barns (determined by nuclear magnetic resonance measurements).

Using equation (9) with the eigenvalues (10) of  $\mathbf{Q}_{zz}$ , the eigenvalues of  $\mathbf{H}_Q$  for the quadrupole energy shifts become:

**Quadrupole energy shift:** 
$$\Delta E_Q = \frac{eQ}{4} \frac{\partial^2 \phi_E}{\partial z^2} \left[ \frac{3I_z^2 - I(I+1)}{I(2I-1)} \right] \quad (11)$$

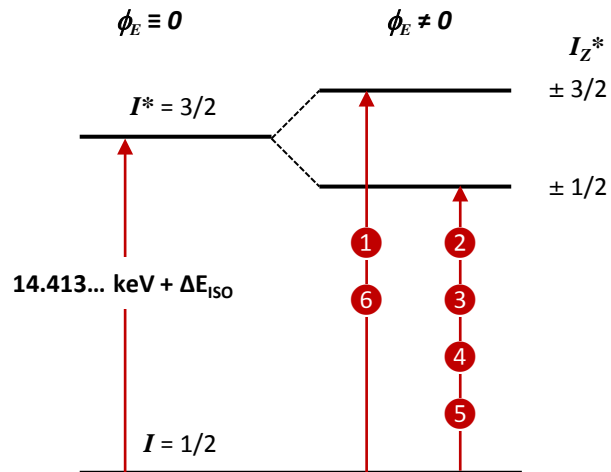
The  $^{57}\text{Fe}$  ground state has  $I = 1/2$ , so its  $\mathbf{Q} \equiv 0$  and  $\therefore \Delta E_Q \equiv 0$ . The 14.4keV excited state has  $I^* = 3/2$ , so it has two different  $\Delta E_Q$  eigenvalues:

$$\begin{aligned} I_z^* = \pm \frac{3}{2}: \quad \Delta E_Q &= + \frac{eQ}{4} \frac{\partial^2 \phi_E}{\partial z^2} \\ I_z^* = \pm \frac{1}{2}: \quad \Delta E_Q &= - \frac{eQ}{4} \frac{\partial^2 \phi_E}{\partial z^2} \end{aligned} \quad (12)$$

The resulting quadrupole splitting of the 14.4keV state is diagrammed in Figure 5 on page 9.

Quadrupole energy shifts can occur along with hyperfine shifts, in which case the two outer hyperfine lines are both shifted oppositely to the shifts of the remaining four lines. The direction of this relative shift of the outer two lines indicates the sign of  $\partial^2 \phi_E / \partial z^2$  (where the  $z$ -axis is defined by the direction of  $\vec{B}$  causing the hyperfine splitting): a relative shift of lines 1 and 6 to higher energy would indicate that  $\partial^2 \phi_E / \partial z^2 > 0$ .

Figure 5: Quadrupole splitting of the  $^{57}\text{Fe}$  14.4keV nuclear absorption line in an electric field which is not spherically symmetric. Magnetic dipole selection rules again require that  $\Delta I_z = \pm 1$  or 0 for this gamma-ray transition, and the numbers on the arrows correspond to those numbers shown for the six hyperfine transitions in Figure 2 on page 4. The direction of the splitting of the 14.4keV state shown here assumes that  $\partial^2 \phi_E / \partial z^2 > 0$ .



## EXPERIMENTAL APPARATUS

### *Motion control, source, absorber, detector*

Unlike the apparatus in Experiment 28, in this experiment the apparatus moves the  $^{57}\text{Co}$  source while the absorber remains stationary. As diagrammed in Figure 6, the source is attached to a solenoid controlled by an electronic feedback and control unit, which oscillates the source toward and away from the absorber and detector while monitoring its position. As we will use the system, the solenoid will give the source a constant acceleration for  $\frac{1}{2}$  of each cycle, changing the acceleration direction half way through each cycle. Because the acceleration of the source is constant for half of each cycle, the velocity of the source increases and decreases

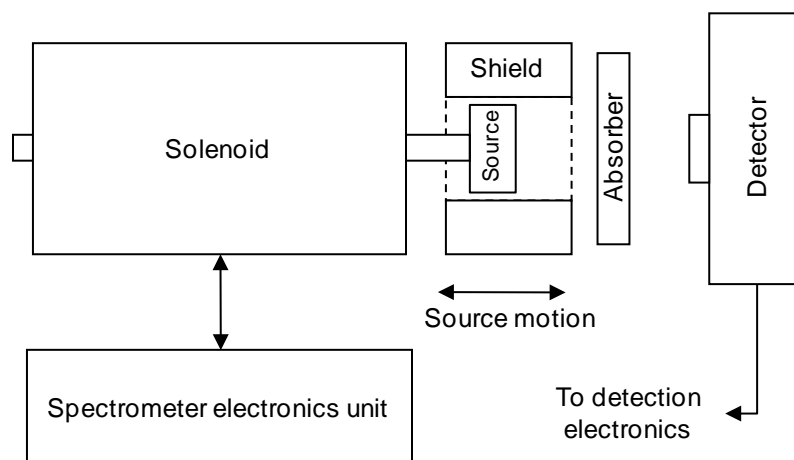
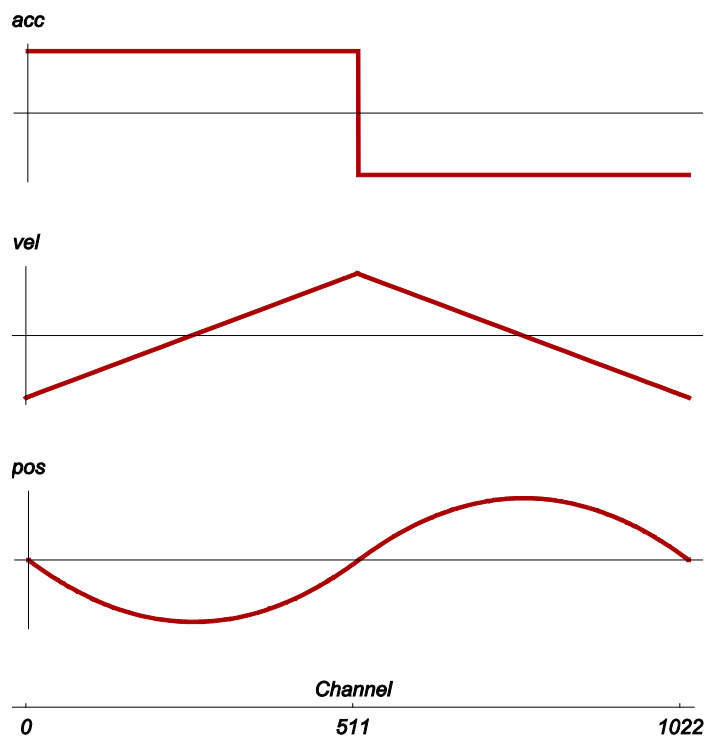


Figure 6: General arrangement of the Mössbauer source, absorber, and detector hardware. The solenoid drives the motion of the source; its design is similar to that of the voice-coil in a loudspeaker.



**Figure 7: The relation between source acceleration, velocity, position, and spectrum channel number. Velocity is + for motion of the source toward the absorber; position is + when the source is closer to the absorber.**

linearly, as shown in Figure 7. Each velocity is therefore sampled twice during a single cycle: as the velocity increases (channels 0-511) and again as the velocity decreases (channels 512-1022). Unfortunately, this apparatus does not provide a calibrated velocity or position readout, so you will use a natural iron Mössbauer spectrum to calibrate the channel velocities.

### ***14.4KeV gamma detection electronics***

As was the case in Experiment 28, the detector is a gas-proportional counter with a preamp mounted close to it. The detector's associated electronics units are diagrammed in Figure 8 on page 11. The detector's high voltage is controlled by a power supply mounted in the equipment rack. The output of the preamp is further amplified and fed to a *single channel analyzer* (SCA), which will generate a digital output pulse whenever an amplifier output pulse has an amplitude that falls within its adjustable discriminator window. You will set the SCA window upper and lower levels to respond to detections of the 14.4 KeV gamma ray we use for Mössbauer spectroscopy. By using a digital oscilloscope connected to the amplifier output but triggered by the SCA output, you can see the amplified pulses that fall within the discriminator settings of the single channel analyzer. You will use the oscilloscope to adjust the SCA discriminator window to accept only the 14.4 KeV gammas. The other oscilloscope monitors the source position output provided by the Mössbauer spectrometer unit.

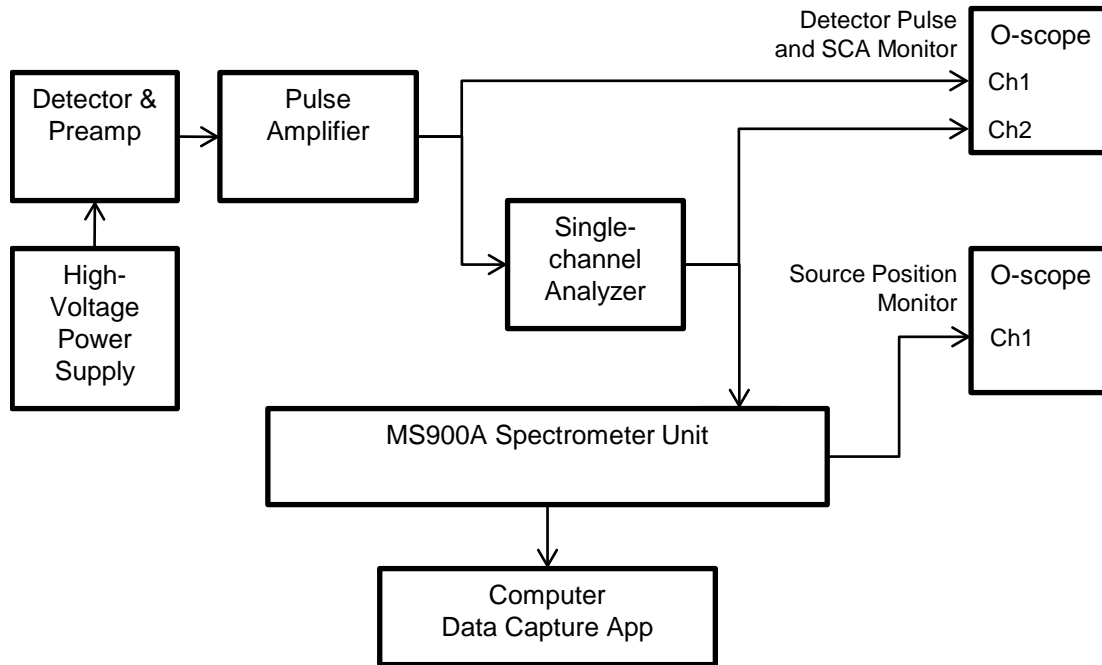


Figure 8: Block diagram of the detector and acquisition electronics units.

*Spectrometer unit front-panel controls*

The heart of the apparatus is a commercial Mössbauer spectrometer, a Ranger Scientific MS900A. Figure 9 shows the front panel of the MS900A and how its controls should be configured. The **SAMPLING TIME** must be set to “20.1” (200 microseconds) or the computer data capture application will not work properly. The **TIME** button must be deselected (out) for the data capture software to properly calculate the spectrum acquisition time.

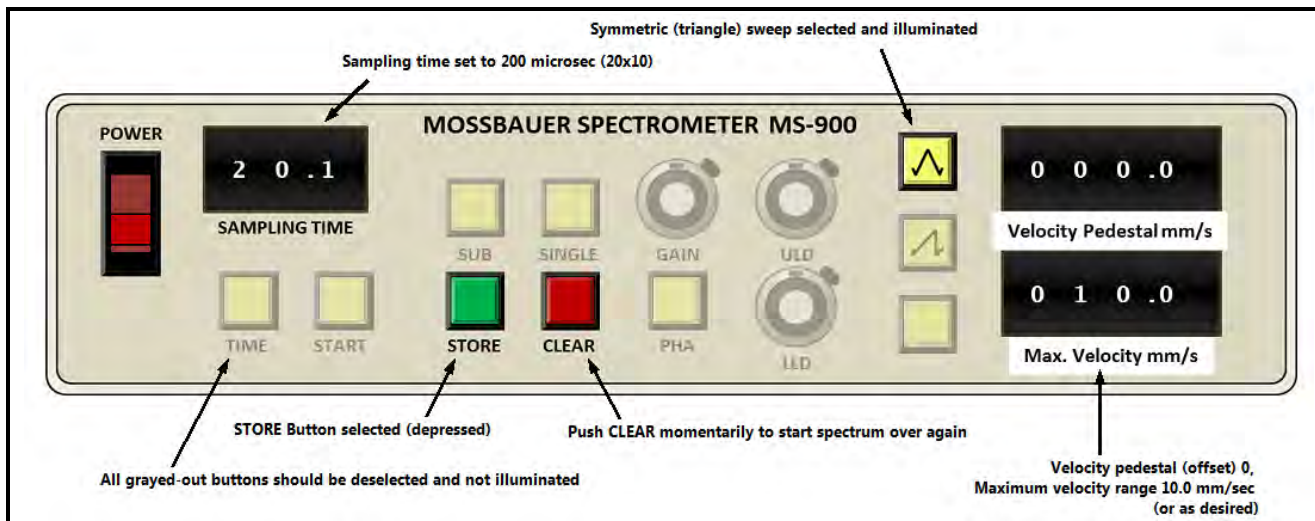


Figure 9: Front panel of the MS900A spectrometer control electronics and recommended settings.

The primary MS900 controls you will use as you perform the experiment are the **STORE** and **CLEAR** buttons:

**STORE:** push to enable, push again to disable. When enabled (selected, depressed in), a spectrum histogram is collected and continually updated with each oscillation of the source position. When disabled (out), the spectrum histogram is held in memory unchanged.

**CLEAR:** push momentarily (a second or two) to erase the histogram memory. When released, a new spectrum will be collected (if the **STORE** button is enabled).

Other controls of note:

**Sweep type:** The symmetric (triangle) sweep type button should be selected and illuminated.

**Max. Velocity:** Set this control to determine the velocity range of the source oscillation. 10 mm/sec (shown in Figure 9) is an appropriate range for the absorbers you will use.

### *Absorbers*

**Stainless Steel:** a nonmagnetic alloy of iron, the same material as is used in Experiment 28. Because this absorber will produce a spectrum with only a single absorption line, it is useful to relatively quickly check the operation of the apparatus.

**Natural Iron:** a foil of pure, metallic,  $\alpha$ -iron. By definition, this absorber has an isomeric shift of 0, and its *bcc* crystal structure exhibits no quadrupole splitting. Its ferromagnetic nature causes a large hyperfine splitting, and the line positions of this spectrum will be used to calibrate your channel velocities.

**Iron(II) Sulfate:** ferrous sulfate ( $\text{FeSO}_4 \cdot \text{H}_2\text{O}$  +  $\text{FeSO}_4 \cdot 7\text{H}_2\text{O}$ ) exhibits quite strong quadrupole splitting. Used to treat iron deficiency, it is on the World Health Organization's *List of Essential Medicines*. Our sample is probably a mixture of mainly the two hydrated forms shown.

**Iron(III) Oxide:**  $\alpha$ -phase ferric oxide ( $\text{Fe}_2\text{O}_3$ ), also known as *hematite* or even “rust,” is weakly ferromagnetic at room temperature, but transitions to antiferromagnetic at 260 Kelvin. It exhibits hyperfine splitting significantly larger than that of metallic iron, and has, in fact, the largest splitting of all the various iron oxides. It exhibits quadrupole shifts as well. It was once the most commonly used material for magnetic tape and disc storage media.

### *Data capture software*

The spectrum information is completely controlled by the MS900A unit. It is interfaced to a computer using a standard lab data acquisition system through an appropriately configured DAQ interface box. The interface application, **MS900 Data Capture**, only serves to copy and display the current spectrum histogram data transmitted by the MS900 over its computer interface cable.

The data capture application can store the histogram data to a standard *CurveFit* data file. The program calculates and displays the accumulated histogram acquisition time (in seconds) and will save this time in the comment section of a data file. The application's user interface is very simple (Figure 10).

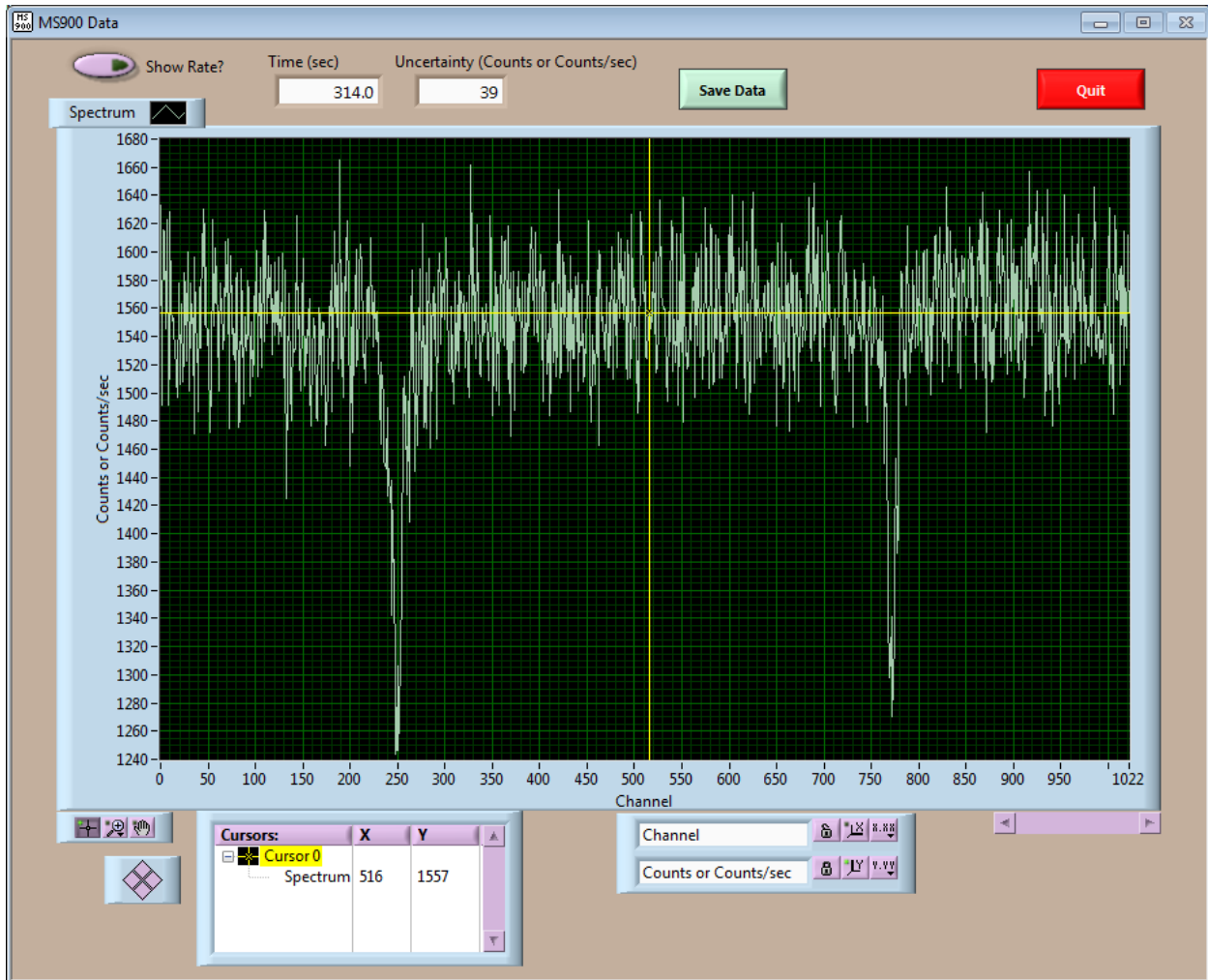


**Figure 10: The MS900 Data Capture application user interface window, displaying a short histogram spectrum of a stainless steel absorber. The main user controls are the *Save Data* and *Quit* buttons. The *Show Rate?* switch converts the displayed histogram data to count rate. Saved file data are always saved in a format of standard *CurveFit* (x,y) pairs: x = channel, y = counts.**

## EXPERIMENTAL PROCEDURE

### *Initial setup*

1. High voltage: 1800V, + polarity
2. Amplifier: Coarse Gain: 200, Shaping Time 2 $\mu$ S, Polarity +
3. Single Channel Analyzer (SCA): Upper Level: 5.00, Lower Level: 0.00
4. MS-900: Sampling time: 20.1 (200  $\mu$ s); Velocity Pedestal: 0.0; Max Velocity: 10.0
5. Upper (Pulse) oscilloscope: Trigger CHAN 2 (the SCA output)

Remove any absorbers or lead shielding between the source and the detector. Apply the high voltage to the detector. Use the pulse oscilloscope display and the X-ray filter to identify the 6 keV and 14.4 keV pulses from the amplifier. Trigger the oscilloscope on the SCA output pulses and adjust the SCA levels until only 14.4 keV pulses trigger the SCA output (Figure 11).

6. MC900A source velocity profile: symmetric (triangular)

Start the *MS900 Data Capture* application. The program will initially display a window with a diagram of the MS900 front panel showing the proper control settings (as in Figure 9 on page 11). Close this MS900 setup window by clicking the mouse cursor anywhere on it. With the proper source motion selected, the lower oscilloscope should display the oscillating position profile of the source.

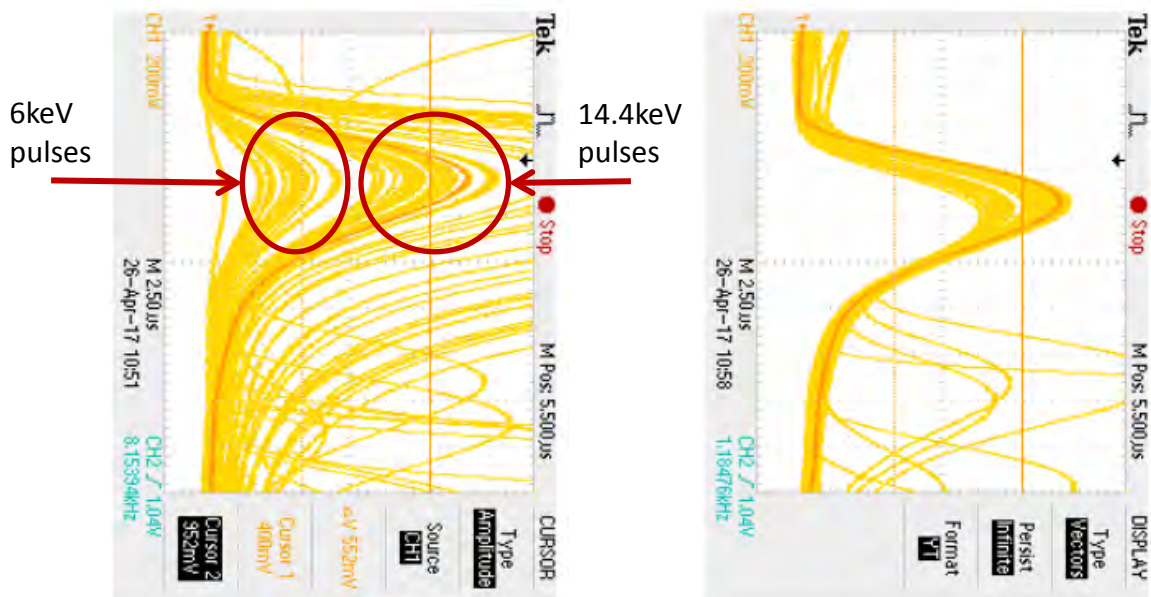


**Figure 11: Typical oscilloscope displays of the amplifier pulse output. Left: SCA upper and lower level discriminators opened to show all pulses. The bands of pulse heights associated with 6keV and 14.4keV photon detections are shown. Right: SCA upper and lower level discriminators set to include only the 14.4keV photon detections.**



### *Spectrum acquisitions*

**Stainless Steel:** insert the stainless steel absorber first. Use the X-ray filter to help secure the absorber to the sample shelf. Turn on the MS900 **STORE**, and push and hold the MS900 **CLEAR** until the computer-displayed spectrum resets. After a few minutes the displayed spectrum should begin to show absorption lines near channels 256 and 768. When you can clearly identify the absorption lines (after about 10 minutes), save the spectrum using the data capture application. Don't waste a lot of time collecting this spectrum once you can identify the absorption line. If the absorption lines don't appear, then you probably don't have the SCA window set properly or you've set up the MS-900 incorrectly.

**Natural Iron:** once you have obtained a useable stainless steel spectrum replace the absorber with a natural iron sample and **CLEAR** the MS-900 spectrum. **Collect this spectrum for at least 90 minutes** because you want a high-quality spectrum of the iron. The line positions of this spectrum will be used to calibrate your channel velocities.

**Iron(II) Sulfate:** ferrous sulfate ( $\text{FeSO}_4$ ) exhibits only quadrupole splitting. Use most of the remaining lab time to collect a spectrum of the iron sulfate sample.

**Iron(III) Oxide:** Set up the ferric oxide ( $\text{Fe}_2\text{O}_3$ ) sample to collect a spectrum overnight. Ferric oxide exhibits hyperfine splitting along with quadrupole shifts.

## DATA ANALYSIS

The primary tools you will need for your data analysis are *CurveFit*, the *Mosspec.nb* notebook, found in the website directory:

[http://www.sophphx.caltech.edu/Physics\\_7/Mathematica\\_Notebooks/Mosspec\\_Exp\\_29/](http://www.sophphx.caltech.edu/Physics_7/Mathematica_Notebooks/Mosspec_Exp_29/)

and, most importantly, your brain.

Each complete spectrum data set contains two independent images of the spectrum, because during each cycle of the source's motion, the source experiences a given velocity twice. Figure 12 shows an example of a complete natural iron data set showing the two spectrum images. The velocity goes from maximally negative at channel 0 to maximally positive near channel 511, then back to maximally negative at channel 1022. The source passes through 0-velocity near channels 256 and 768. It is farthest from the detector near channel 256 and closest near channel 768, as illustrated in Figure 7 on page 10. Consequently,

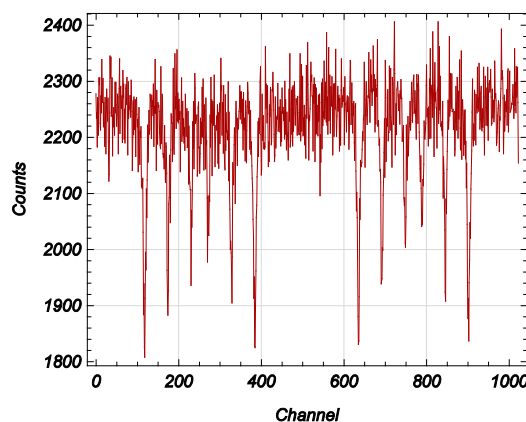


Figure 12: A MS900 spectrum of  $\alpha$ -iron.

the 6 natural iron hyperfine absorption lines are visible in both the upper and lower halves of the data set. The count data in each channel are subject to Poisson count statistics, naturally, so you will assign the appropriate uncertainties to the count data. *CurveFit* and the *Mosspec.nb* notebook have functions to assign these uncertainties for you.

### *Channel velocity calibration*

You will use your natural iron spectrum to calibrate the channel velocities of both the upper and lower halves of a spectrum. Calibration consists of using the known natural  $^{57}\text{Fe}$  line velocities to determine the 0-velocity channel and the velocity increment per channel. Each spectrum half (channels 0–511 and 512–1022) must be calibrated separately. *Mosspec.nb* provides a palette interface which makes this process straightforward. The steps for a full calibration are:

1. If using the website link above to find *Mosspec.nb*, you must first save a copy of the notebook to your computer. Launch the *Mosspec.nb* notebook using *Mathematica*®, and execute the notebook's initialization cells. *CurveFit* should start and an additional **Mosspec** palette should appear on the left side of the display.
2. Load your  $\alpha$ -Fe data set (**Load Mosspec File** palette button).
3. Assign Poisson uncertainties to the count data (**Set to Poisson count data** button).
4. Select a data subset which includes only the Fe spectrum occupying the lower half of the velocity channels (**Keep an X-range** button).

5. Use the known  $\alpha$ -Fe line velocities to calibrate this half of the channels (**Calibrate** button). Check the  $\chi^2$  and the fit results plot to make sure the calibration correctly located the 6 iron lines and is accurate. If not, try rebinning the data (**Rebin Data** button) and attempt to calibrate again. The program will perform a linear fit of the observed line positions (in channel number) to the known  $\alpha$ -Fe line velocities (in mm/sec). It will save this calibration formula for use with other spectra you load.
6. Convert the channel numbers ( $x$ -axis) to velocities (**Convert to Velocity** button). The  $x$ -axis scale in the data plot should now be in mm/sec. If so, the velocity calibration of the lower channels is complete.
7. Restore the full Fe line spectrum (result following step 3) by pushing the **Undo** palette button a couple of times.
8. Now select the upper half of the channel spectrum (**Keep an X-range** button) and calibrate it (steps 5 and 6).

*Mosspec* maintains these two independent channel calibrations, one for each half of the spectrum. Its `VelocityParameters[ ]` function gives you access to the calibration coefficients. Use the *Mosspec* palette **Help** button to see a notebook with a list of the available functions. Clicking on one of the functions listed will then give its description.

### *Fitting the absorption lines of a Mössbauer spectrum*

Once you have calibrated using  $\alpha$ -Fe, you can load another spectrum, assign Poisson uncertainties, then and window the data to look at either half of it (as in steps 2–4 of the velocity calibration). Clearly, each Mössbauer spectrum acquired using the MS900 contains two complete, independent data sets. You used your  $\alpha$ -Fe spectrum to independently velocity-

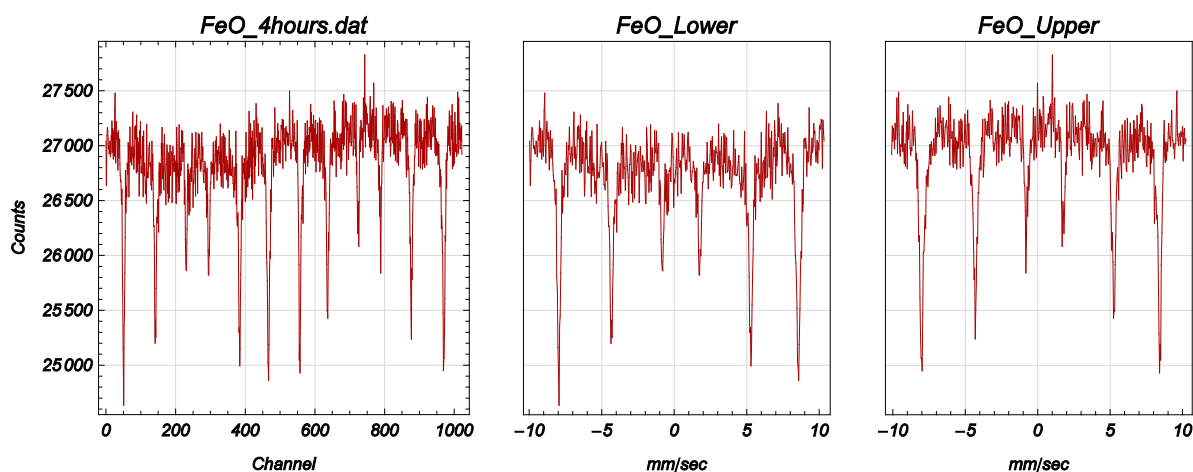


**Figure 13:** A raw MS900 Mössbauer spectrum contains two independent data sets (in this case of  $\text{Fe}_2\text{O}_3$ ). Using your  $\alpha$ -iron spectrum to determine the velocities corresponding to the spectrum channels, you can convert each half of the raw spectrum into a spectrum of absorption lines vs. velocity, as shown in the center and right graphs.

calibrate each half of the spectrum channel set (0–511 and 512–1022). Given these two independent calibrations, another acquired Mössbauer spectrum yields two independent, calibrated absorption line vs. velocity spectra, as shown in Figure 13. Use the **Convert to Velocity** button to convert the selected half of a spectrum's  $x$ -axis to velocity using your previous natural Fe velocity calibration.

Once converted to velocities, you can fit the lines of the selected half of the spectrum using the appropriate *Mosspec* **Fit Lines** button. Make sure you carefully examine the results (including a plot of the fit results) to make sure the lines were identified correctly by the program. Rebinning the data or providing initial line position estimates to the `FitLines[ ]` function may be necessary if the lines are weak and noisy. If successful, the fitting function will return the resulting line velocities in mm/sec and with their uncertainties, along with other parameters. You should include *CurveFit* plots of the fit results and the resulting fit parameters with your analysis.

### *Analyzing the absorption line velocities*

You should separately analyze each of the two halves of the complete, raw Mössbauer spectrum. By comparing the two results, you may be able to say something about the magnitudes of various systematic errors which are not reflected in the results' individual uncertainty estimations (for example, nonlinearity in the actual channel-to-velocity function not included in the velocity calibration result).

The number and positions of the various absorption lines of a spectrum are determined by the various perturbations to the energy of the 14.4keV transition discussed previously: *isomeric shift*, *hyperfine splitting*, and *quadrupole splitting*. The measured radial velocity of a line determines its energy shift using equation (2) on page 2; the energy shifts  $\Delta E_B$  of each level due to hyperfine splitting are described by equation (4) on page 3; the quadrupole shifts  $\Delta E_Q$  in the excited state levels by equations (11) and (12) on page 8. The isomeric shift  $\Delta E_{iso}$  is determined from an average of the positions of all lines. Since you are measuring velocities for line positions rather than energy shifts, use the relation:

$$\Delta v_{I_z, I_z^*} = v_{iso} + v_B \left[ I_z - \frac{g^*}{g} I_z^* \right] + v_Q \left[ (I_z^*)^2 - \frac{5}{4} \right] \quad (13)$$

Expressions relating the hyperfine and quadrupole shift velocities to the relevant atomic and nuclear parameters are derived in Prelab Problems 2 and 3.

If the spectrum contains only one line (stainless steel), then  $v_B$  and  $v_Q$  are both too small to lead to observable line splitting. Of course, any spectrum should provide a measurement of the absorber's isomeric shift  $v_{iso}$ . Is the stainless steel isomeric shift consistent with what you measured in Experiment 28? What about the stainless steel line width?

If exactly two lines are visible, then  $\nu_Q$  is clearly nonzero ( $\text{FeSO}_4$ ). Given an excited state quadrupole moment of  $Q = +0.082$  barns, use your measured line splitting (**Fit 2 Lines** button) to determine the magnitude of  $e \partial^2 \phi_E / \partial z^2$  (in  $\text{eV}/\text{\AA}^2$ ) for  $\text{FeSO}_4$ .

A 6-line spectrum implies that  $\nu_B$  and  $(g/g^*)$  may be measured from the line velocities, and a nonzero  $\nu_Q$  may be measureable as well. *Mosspec.nb* provides a function to fit the line velocities of a 6-line spectrum to the theoretical model given in equation (13). Once you have fit the lines (**Fit 6 Lines** button) of your  $\text{Fe}_2\text{O}_3$  spectrum (and your Fe spectrum), you then use the **Model 6 Lines** palette button to perform the analysis. Carefully examine the results of the line fits, including the  $\chi^2$  as well as the uncertainties in the model parameters. Note also the differences between the model's predicted line velocities and the line velocities determined from the data. You should model both the lower and upper halves of the spectrum. Are the model fit results consistent with each other given the  $\chi^2$  values and the uncertainties? What do you conclude is your measured value of  $(g/g^*)$ ? Calculate ambient  $B$  fields (with uncertainties, of course) from the measured  $\nu_B$  values and  $e \partial^2 \phi_E / \partial z^2$  from the measured  $\nu_Q$  values.

What about the Fe and  $\text{Fe}_2\text{O}_3$  line widths? How do they compare to the natural line width you calculated from the excited state's half-life (Experiment 28 prelab problems)? Note that the **FitLines[]** function uses a single line width to fit all lines it finds. This may not be a very good idea for the multi-line spectra. You can always select a single absorption line (using the **Keep an X-range** button) and then fit it with a single line (**Fit 1 Line** button). Do this for an inner and an outer line of one of your 6-line spectra. How do the widths of the two lines compare?

### *Merging the two halves of a spectrum into a single data set*

Here is a procedure to combine both halves of a spectrum into a single, merged data set:

1. Select one half of the full spectrum and convert the  $x$ -axis to velocities.
2. Save this spectrum using the *CurveFit* main palette **Undo and Backup: Backup data** button and menu selection. By doing this, you can later merge this data with that for the other half of the acquired spectrum.
3. Select the other half of the spectrum and again convert its  $x$ -axis to velocities.
4. Merge the first, backed-up spectrum using the *CurveFit* main palette **Undo and Backup: Merge Backup with data** button and menu selection.

This procedure may be especially useful to improve the quality of your data for a spectrum taken for only a few minutes.

## PRELAB PROBLEMS

1. Ferromagnetic materials typically have a single unpaired electron per atom whose magnetic moment contributes to the ambient, average magnetic flux density  $B$  present in a typical magnetic domain. The magnitude of the magnetic dipole moment  $\vec{m}$  of a single electron is approximately equal to a *Bohr magneton*:  $\mu_B = 5.79 \times 10^{-5}$  eV/Tesla. The *number density* of iron atoms in its  $\alpha$ -iron phase is given by Avogadro's number divided by iron's molar volume:  $n_{\text{Fe}} = 0.85 \times 10^{23} / \text{cm}^3$  (note that this is typical of the atomic number density of many materials:  $\approx 10^{23} / \text{cm}^3$ ). The average magnetic flux density  $B$  produced within a typical domain of a magnetic material with an average magnetic dipole density  $\vec{M}$  (all aligned in the same direction) is approximately given by  $B \approx \mu_0 M$ , where  $\mu_0 = 4\pi \times 10^{-7}$  (meter<sup>3</sup>Tesla<sup>2</sup>/Joule) is the *vacuum permeability*. What is the approximate average magnetic flux density  $B$  within a domain of ferromagnetic iron (assuming  $1\mu_B$  per atom)?

Note: you can use *Mathematica*® expressions to provide these numbers (assuming version 9 or later):

```
 $\mu_B$ : UnitConvert[ Quantity["BohrMagneton"], ("Electronvolts"/"Teslas") ]
 $\mu_0$ : UnitConvert[ "MagneticConstant", ("Meters"^3 "Teslas"^2/"Joules") ]
 $n_{\text{Fe}}$ : UnitConvert[ (UnitConvert[ Quantity[ 1,"AvogadroConstant" ] ] /
                    ElementData[26,"MolarVolume"],
                    "Centimeters"^(3) ]
```

2. For an absorber exhibiting *hyperfine splitting only* (no quadrupole and isomeric shifts), show that the relative velocity of the line representing the transition between the  $^{57}\text{Fe}$  ground state  $|I, I_z\rangle$  and the 14.4keV excited state  $|I^*, I_z^*\rangle$  can be written as:

$$\Delta v_{I_z, I_z^*} = v_B \left[ I_z - \frac{g^*}{g} I_z^* \right] \quad (14)$$

What is the expression for  $v_B$  in terms of  $g$ ,  $\mu_n$ ,  $B$ , and  $E_0$ ? Equation (2) on page 2 and (4) on page 3 may be helpful. Given  $g = +0.1809$  and  $\mu_n = 3.15 \times 10^{-8}$  eV/Tesla, calculate the value of  $v_B/B$  in (mm/sec)/Tesla. (answer: 0.1186)

For a 1 Tesla field, what is the expected velocity separation (in mm/sec) between lines 1 and 6 (see Figure 2 on page 4) if  $g^*/g = -1/1.75$ ? (answer: 0.322 mm/sec)

Again note: you can use *Mathematica*® expressions to provide the relevant numbers (assuming version 9 or later):

```
 $\mu_n$ : UnitConvert[ Quantity["NuclearMagnetons"], ("Electronvolts"/"Teslas") ]
 $E_0$ : UnitConvert[ (IsotopeData["Fe57", "ExcitedStateEnergies"]//First), "Electronvolts" ]
 $g$ : 2 IsotopeData["Fe57", "MagneticMoment"] / Quantity["NuclearMagnetons"]
 $c$ : 1.0 UnitConvert[Quantity["SpeedOfLight"], "Millimeters"/"Seconds"]
```

3. For an absorber exhibiting *quadrupole splitting only* (no hyperfine splitting or isomeric shift), show that the shift in velocity of a line representing the transition between the  $^{57}\text{Fe}$  ground state  $|I, I_z\rangle$  and the 14.4keV excited state  $|I^*, I_z^*\rangle$  can be written as:

$$\Delta v_{I_z, I_z^*} = v_Q \left[ (I_z^*)^2 - \frac{5}{4} \right] \quad (15)$$

Consider equations (11) and (12) on page 8. Give an expression for  $v_Q$  in terms of the atomic and nuclear properties used in those expressions.

4. Find *Mosspec.nb* on the lab network drive and copy it to your computer. Open it using *Mathematica*® and ensure that the initialization cells are executed. Use the command:

**ModelPeaks[ FeLineV[ ] ]**

to determine the velocity parameters  $v_{iso}$ ,  $v_B$ , and  $v_Q$  from a fit of equation (13) on page 18 to a list of the standard  $\alpha$ -iron line velocities (executing **FeLineV[ ]** alone returns a list of these velocities).

- a. What is the average line velocity uncertainty according to the fit results?
- b. From the fit's value for  $v_B$ , what must be the ambient magnetic flux density  $B$  (in Tesla) at the location of an iron nucleus?
- c. How does the fit's calculation of  $(g/g^*)$  compare to the value given in the text to be  $-1.752$ ?